Experimental Neurology 261 (2014) 53–64

Contents lists available at ScienceDirect

Experimental Neurology

journal homepage: www.elsevier.com/locate/yexnr

Regular Article

Intranasally administered mesenchymal stem cells promote a regenerative niche for repair of neonatal ischemic brain injury

Vanessa Donega [a], Cora H. Nijboer [a], Geralda van Tilborg [b], Rick M. Dijkhuizen [b], Annemieke Kavelaars [c], Cobi J. Heijnen [a,c,*]

[a] Lab. of Neuroimmunology and Developmental Origins of Disease, University Medical Center Utrecht, Utrecht, The Netherlands
[b] Biomedical MR Imaging and Spectroscopy Group, Image Sciences Institute, University Medical Center Utrecht, The Netherlands
[c] Lab. of Neuroimmunology, Department of Symptom Research, The University of Texas, MD Anderson Cancer Center, Houston, TX, USA

ARTICLE INFO

Article history:
Received 18 February 2014
Revised 30 May 2014
Accepted 9 June 2014
Available online 16 June 2014

Keywords:
Neonatal hypoxia–ischemia
Nasal MSC therapy
Microglia polarization
Neurogenesis
Neuroregeneration
Scar formation

ABSTRACT

Previous work from our group has shown that intranasal MSC-treatment decreases lesion volume and improves motor and cognitive behavior after hypoxic–ischemic (HI) brain damage in neonatal mice. Our aim was to determine the kinetics of MSC migration after intranasal administration, and the early effects of MSCs on neurogenic processes and gliosis at the lesion site.

HI brain injury was induced in 9-day-old mice and MSCs were administered intranasally at 10 days post-HI. The kinetics of MSC migration were investigated by immunofluorescence and MRI analysis. BDNF and NGF gene expression was determined by qPCR analysis following MSC co-culture with HI brain extract. Nestin, Doublecortin, NeuN, GFAP, Iba-1 and M1/M2 phenotypic expression was assessed over time.

MRI and immunohistochemistry analyses showed that MSCs reach the lesion site already within 2 h after intranasal administration. At 12 h after administration the number of MSCs at the lesion site peaks and decreases significantly at 72 h. The number of DCX^+ cells increased 1 to 3 days after MSC administration in the SVZ. At the lesion, $GFAP^+$/$nestin^+$ and DCX^+ expression increased 3 to 5 days after MSC-treatment. The number of $NeuN^+$ cells increased within 5 days, leading to a dramatic regeneration of the somatosensory cortex and hippocampus at 18 days after intranasal MSC administration. Interestingly, MSCs expressed significantly more BDNF gene when exposed to HI brain extract *in vitro*. Furthermore, MSC-treatment resulted in the resolution of the glial scar surrounding the lesion, represented by a decrease in reactive astrocytes and microglia and polarization of microglia towards the M2 phenotype.

In view of the current lack of therapeutic strategies, we propose that intranasal MSC administration is a powerful therapeutic option through its functional repair of the lesion represented by regeneration of the cortical and hippocampal structure and decrease of gliosis.

Introduction

Encephalopathy caused by neonatal hypoxic-ischemic (HI) brain injury results in cerebral tissue loss leading to long-term neurological deficits *e.g.* mental retardation and motor impairment (De Haan et al., 2006; Ferriero, 2004; Graham et al., 2008; van Handel et al., 2007; Volpe, 2001).

The capacity of stem cells to treat neonatal encephalopathy is gaining support from an increasing number of studies (Bacigaluppi et al., 2009; Daadi et al., 2010; Donega et al., 2013a; Lee et al., 2010; Pimentel-Coelho et al., 2010; Titomanlio et al., 2011; Yasahura et al., 2008; van Velthoven et al., 2010, 2011, 2013). These studies describe the therapeutic potential of intracranially and intravenously delivered neural stem cells (NSCs) or mesenchymal stem cells (MSCs) in rodent models of neonatal HI or neonatal stroke. We have shown recently that both intracranial and intranasal MSC-treatment at 10 d after HI in neonatal mice significantly decreases cerebral lesion volume and improves long-term motor and cognitive behavior (Donega et al., 2013a; van Velthoven et al., 2010).

In view of the therapeutic potential of non-invasive intranasal MSC administration, we investigated the mechanism underlying MSC-mediated repair. Firstly, we studied the kinetics of MSC migration to the lesion site after intranasal administration. To visualize the arrival of MSCs in the brain, we used fluorescence microscopy and Magnetic Resonance Imaging (MRI). We determined the short- and long-term effects of MSCs on regeneration of the lesion by systematic quantification and characterization of precursor cells (type B cells; uncommitted

* Corresponding author at: Lab of Neuroimmunology, Department of Symptom Research, The University of Texas, MD Anderson Cancer Center, 1515 Holecombe Blvd, Unit 384, FCT11.5060, Houston, TX 77030-4009, USA.
E-mail address: CJHeijnen@mdanderson.org (C.J. Heijnen).

http://dx.doi.org/10.1016/j.expneurol.2014.06.009

precursors), neural progenitor cells (type A cells; neuronally-committed), neurons, microglia and astrocytes.

Material and methods

Ethics statement

Experiments were performed according to the international guidelines from the EU Directive 2010/63/EU for animals experiments and approved by the Experimental Animal Committee Utrecht (University Utrecht, Utrecht, Netherlands).

Animals

Unilateral HI brain damage was induced in 9 day old C57BL/6 mice (Harlan Laboratories, The Netherlands) by permanent occlusion of the right common carotid artery under isoflurane anesthesia followed by hypoxia (45 min at 10% oxygen). Sham-controls underwent anesthesia and incision only.

MSCs were purchased from Invitrogen (GIBCO mouse C57BL/6 MSCs, Life Technologies, UK) and cultured according to the manufacturer's instructions. Characterization of cell specific antigens has been described previously by us (van Velthoven et al., 2011). Before administering 1×10^6 MSCs intranasally, each nostril was treated with 3 μL of hyaluronidase (100 U, Sigma-Aldrich, St. Louis, MO) in PBS to increase the permeability of the nasal mucosa. Thirty minutes later, pups received 3 μL of MSCs or PBS (vehicle) twice in each nostril.

Histology

Coronal paraffin sections (8 μm) of paraformaldehyde (PFA)-fixed brains were incubated with mouse-anti-myelin basic protein (MBP) (Sternberger Monoclonals, Lutherville, MD,) or mouse-anti-microtubule-associated protein 2 (MAP2) (Sigma-Aldrich) followed by biotinylated horse-anti-mouse antibody (Vector Laboratories, Burliname, CA). Binding was visualized with Vectastain ABC kit (Vector Laboratories) and diaminobenzamidine.

Immunohistochemistry

MSCs were labeled with PKH-26 Red Fluorescent Cell Linker Kit (Sigma-Aldrich). Coronal frozen sections (8 μm) were incubated overnight at 4 °C with primary antibodies; goat anti-DCX (1:300) (Santa Cruz Biotechnology, TX, USA), rabbit anti-Iba1 (1:500) (Wako Chemicals, Osaka, Japan), mouse anti-GFAP (1:100) (Acris antibodies, Herford, Germany), mouse anti-NeuN (1:200) (Chemicon, Temecula, CA), mouse anti-nestin (1:200) (BD Biosciences, Breda, The Netherlands), rat anti-CD16/CD32 (1:300) (BD Pharmingen, Breda, The Netherlands), goat anti-CD206 (1:300) (R&D Systems, Abingdon, UK). Primary antibody binding was detected by incubating with corresponding secondary antibodies for 1 h at room temperature (Supplementary Table 1). Nuclei were counterstained with DAPI (Invitrogen, Paisley, UK) and mounted with FluoroSave reagent (Calbiochem, Nottingham, UK). Fluorescent images were captured using an EMCCD camera (Leica Microsystems, Benelux) and Softworx software (Applied Precision, Washington, USA) or an AxioCam MRm (Carl Zeiss, Sliedrecht, The Netherlands) on an Axio Observer Microscope with Axiovision Rel 4.6 software (Carl Zeiss).

MSC labeling for MRI

Culture flasks were coated with Poly-L-Lysine (0.02 mg/mL) before seeding MSCs. 48 h later, MSCs were incubated with 0.01 mg Fe/mL fluorescent micron-sized superpara-magnetic iron-oxide particles (MPIO; 0.86 μm) (Bangs Laboratories Inc., IN, USA) diluted in GlutaMAX DMEM medium (Life Technologies). After 4 h, excessive MPIO particles were removed by washing 4 times with PBS. About 70% of the cells were labeled with MPIO particles. Images were taken on an Axio-Observer microscope (Carl Zeiss Microscopy, Jena, Germany) with Axiovision rel. 4.6 software (Carl Zeiss Microscopy).

MRI

MRI was performed on a 9.4 T horizontal bore preclinical MRI system (Varian Inc., Palo Alto, CA). T_2^*-weighted gradient echo images of cells in agarose were acquired with TR/TE = 1000/15 ms and 100 μm × 100 μm × 200 μm spatial resolution. T_2^*-weighted gradient echo images of *ex-vivo* mouse brain were acquired with TR/TE = 40/15 ms and a voxel size of 75 μm in all directions.

To verify the detectability of MPIO-labeled MSCs with MRI, cells were homogeneously distributed in 0.4% agarose in PBS at concentrations between 0 and 1000 cells/μL. T_2^*-weighted gradient echo images were acquired with a Millipede™ coil (Varian Inc.), using the following parameters: TR = 1 s, TE = 15 ms, flip angle = 90°, 4 averages, field-of-view 25.6 mm × 25.6 mm, matrix size 256 × 256 and slice thickness 0.2 mm. For the detection of MPIO-labeled cells in *ex-vivo* mouse brain, mice were perfused transcardially with 4% PFA at 2 h after MSC-treatment. T_2^*-weighted images were acquired with a 3D GE sequence, with TR = 40 ms, TE = 15 ms, flip angle = 15°, 32 averages, field-of-view = 22 mm × 12 mm × 10 mm and a voxel size of 75 μm in all directions.

MSCs co-culture with brain extracts

10 days after HI- or sham-operation, mice were euthanized by pentobarbital overdose and decapitated, and their brains were removed. The ipsilateral hemisphere was dissected on ice at −2.0–2 mm from bregma and was subsequently pulverized on liquid nitrogen. Dissected brains were dissolved in KO-DMEM medium (Life Technologies) at a final concentration of 150 mg/mL and centrifuged for 10 min at 3000 *g* at 4 °C. Supernatants were collected as 'brain extract' and protein concentration was measured with the protein assay (Bio-Rad, Hercules, CA). MSCs were cultured at a concentration of 40,000 cells per well in a 24 well-plate for 24 h before replacing the medium with knock-out medium containing 1 mg/mL brain extract. RNA was isolated from the MSCs 72 h after culture with brain extracts.

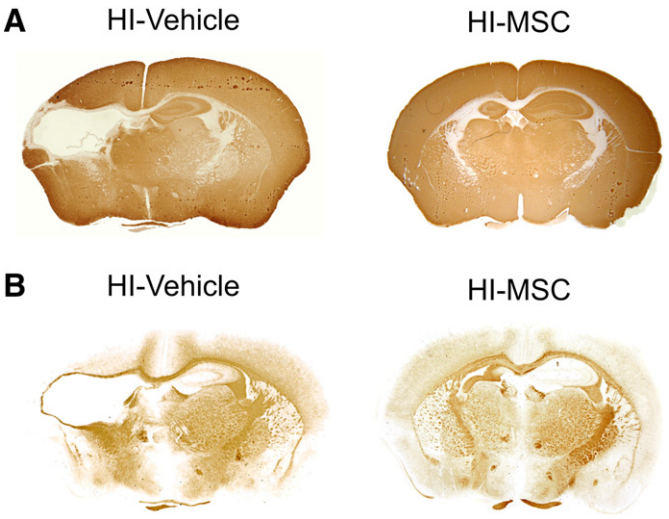

Fig. 1. Intranasal MSC treatment decreases HI lesion size. Representative images of (A) MAP2 and (B) MBP staining from HI-Vehicle and HI-MSC animals at 18 days after MSC administration (*i.e.* 28 days after HI).

RNA isolation and qPCR

Total RNA was isolated with the RNAmini kit according to the manufacturer's instructions (Invitrogen). The amount of RNA was measured with the nanodrop 2000 (Thermo Scientific, Waltham, MA, USA). The RNA quality was determined with the OD 260/280 ratio, which was between 1,9 and 2,1. cDNA was synthetized with SuperScript Reverse Transcriptase (Invitrogen). The expression of BDNF and NGF genes was measured by quantitative reverse transcription (qRT)-PCR (Biorad IQ5, Thermo Scientific) analysis on individual samples. We chose these genes as they are important neurotrophic factors that have been shown to be secreted by MSCs (Crigler et al., 2006). Data was normalized for the expression of GAPDH and actin.

SDS-PAGE gel and Western blot

To assess the expression of BDNF and NGF in sham and HI brain extracts used for co-culture with MSCs, equal amounts of brain extract were loaded on a 15% SDS-PAGE gel (Bio-Rad) and transferred to a nitrocellulose membrane (Hybond C; Amersham Biosciences, Roosendaal, Netherlands). Membranes were blocked with 5% skimmed milk for 1 h, followed by overnight incubation with primary antibodies for rabbit anti-BDNF 1:400 (Santa Cruz Biotechnology, Dallas, Texas) and rabbit anti-NGF 1:1000 (Sigma-Aldrich). Expression was detected by incubation with donkey anti-rabbit-HRP 1:5000 (Amersham Biosciences) and developed by enhanced chemiluminescence (ECL) (Advansta, Isogen Life Science, De Meern, The Netherlands) on a ProXima Imager (Isogen Life Science). To control for equal loading, membranes were reprobed for β-actin followed by donkey anti-goat-HRP 1:5000 (both Santa Cruz Biotechnology).

Data analysis

Analyses were performed in a blinded set-up. PKH-26$^+$ signal was determined by measuring pixel intensity with ImageJ 1.47f Software (Wayne Rasband, National Institutes of Health, USA). Co-localization of GFAP and nestin, CD16/CD32 and Iba-1, CD206 and Iba-1 pixels was assessed with the co-localization macro of ImageJ 1.47f software. GFAP and Iba-1 positive signals were also measured using the ImageJ software. The number of DCX$^+$ and NeuN$^+$ cells was counted manually. Statistical significance in relative mRNA expression was determined with an unpaired two-tailed T-test. Statistical significance between M1 and M2 phenotype was determined by Multiple T-test corrected for multiple comparisons using the Holm–Sidak method. Statistical significance was analyzed using (repeated measures) one-way ANOVA followed by Bonferroni post-tests, when not mentioned otherwise. $p < 0.05$ was considered statistically significant. Data are presented as mean ± SEM. Outliers were identified with the Grubbs test (Q = 2%) or the ROUT test (Q = 2%).

Results

Kinetics of MSC migration to the lesion site

We have previously shown that intranasal MSC treatment significantly decreases HI brain injury at 25 days after MSC treatment (*i.e.* 35 days post-HI) (Donega et al., 2013a). We assessed HI-induced loss of MAP2 and MBP staining as measures for gray and white matter damage, respectively. The results in Fig. 1 confirm our previous data and show that intranasal treatment with 0.5×10^6 MSCs leads to substantial repair of both the somatosensory cortex and hippocampus, which are both severely damaged after HI.

We have shown in a previous study that MSCs administered intranasally to both nostrils, migrate specifically to the ipsilateral side, but not to the contralateral hemisphere (Donega et al., 2013a). To assess the kinetics of MSC migration to the lesion site, we administered PKH-26 labeled MSCs intranasally *via* both nostrils at 10 days after HI. We analyzed sections of the lesion at 2, 6, 12, 24, 48 and 72 h after administration. PKH-26$^+$-MSCs form clusters around the lesion site and appear to home exclusively to the ipsilateral side. Our results show that PKH-26$^+$-MSCs reach the lesion site as early as 2 h after administration and peak at 12 h. At 72 h, the PKH-26$^+$-MSC signal decreases by more than 50% compared to levels at 12 h after administration (Fig. 2).

MRI of MPIO-labeled MSCs

To corroborate our observation that MSCs reach the lesion site within 2 h, we performed *ex-vivo* MRI analysis of mouse brains using MSCs loaded with micron-sized superpara-magnetic iron-oxide particles (MPIO) co-labeled with the fluorescent label Dragon Green. *In vitro* pre-screening of MPIO-labeled MSCs showed a strong fluorescent signal indicating that MSCs had ingested MPIO particles (Fig. 3A). To verify that contrast-induced signal intensity changes represent changes in MPIO-MSC numbers, increasing numbers of MPIO-MSCs were assessed

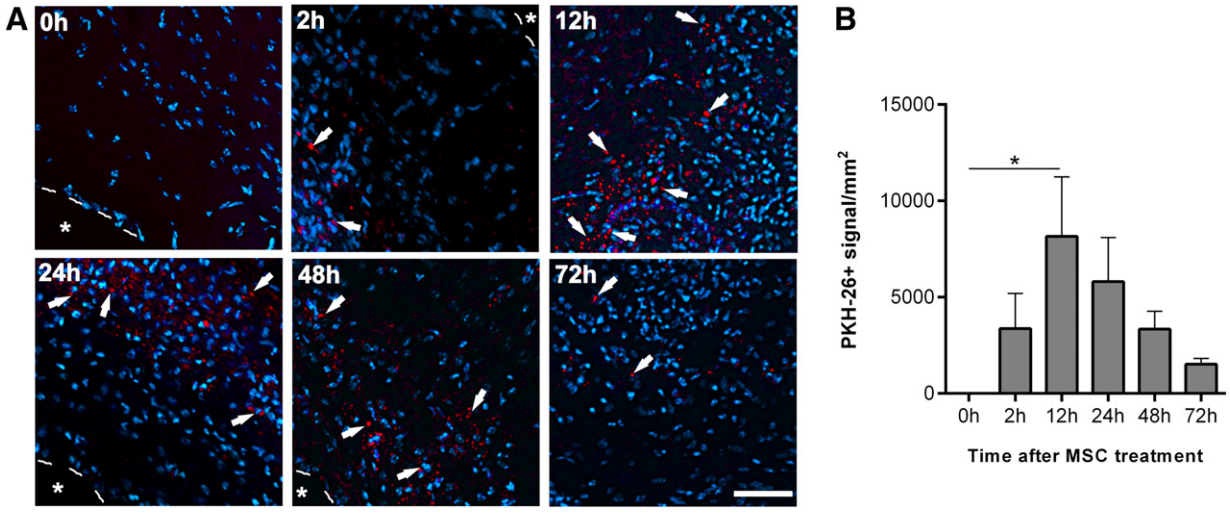

Fig. 2. MSCs reach the lesion site within 2 h after administration. 1×10^6 PKH-26 labeled MSCs were administered intranasally 10 d post-HI. (A) Representative images of PKH-26$^+$ cells (see arrows) at the lesion site at 2, 6, 12, 24, 48 and 72 h following MSC administration. (B) Quantification of PKH-26$^+$ signal/mm^2 at 2, 6, 12, 24, 48 and 72 h. Data represent mean ± SEM. *$p < 0.05$ by ANOVA and Bonferroni post-hoc test (n = 5 per group). Red = PKH-26; blue = DAPI; asterisk = lesion; dashed line = lesion border. Scale bar = 50 μm.

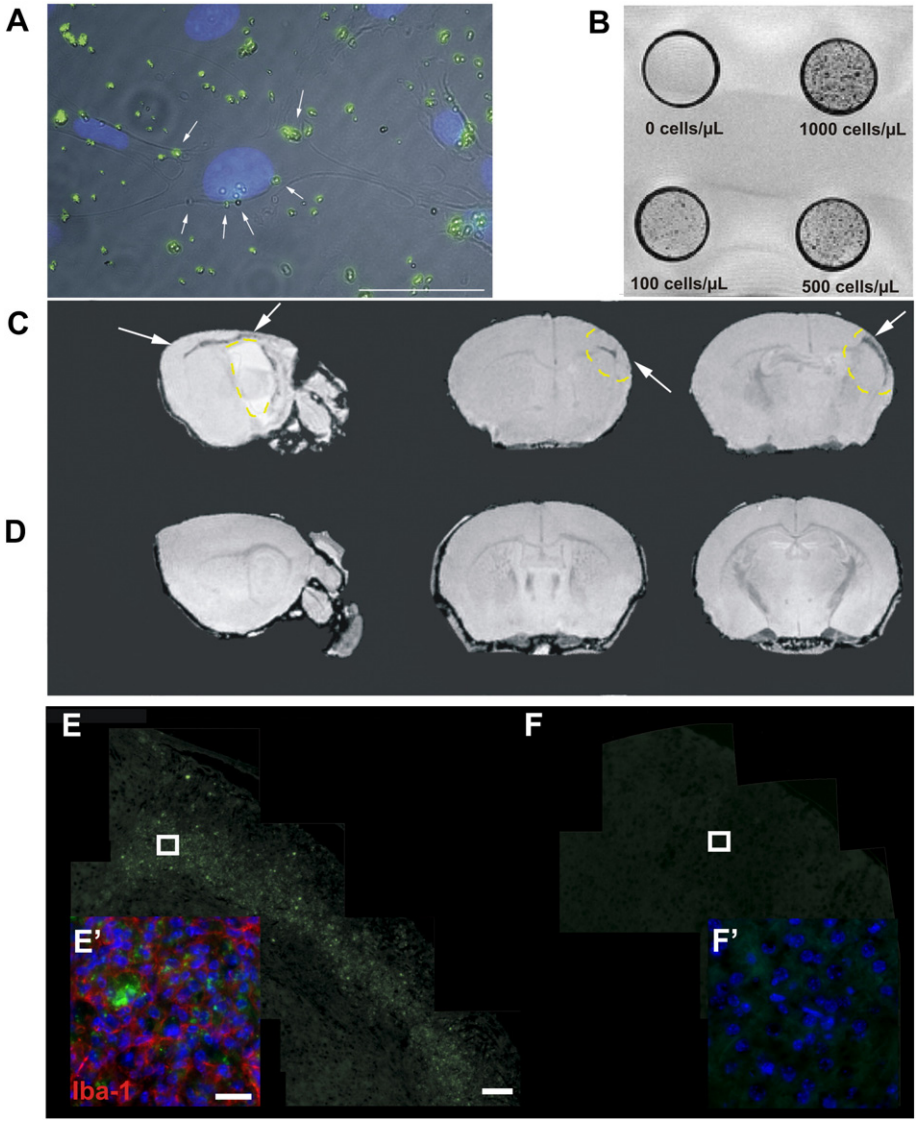

Fig. 3. Magnetic Resonance Imaging of MPIO labeled MSCs. 1×10^6 MPIO-labeled MSCs were administered intranasally at 10 d post-HI or sham-operation. (A) Representative phase-contrast and fluorescent image of MPIO-(Dragon Green) labeled MSCs. Dragon Green MPIOs are taken up by the MSCs. Scale bar = 10 μm. (B) T_2^*-weighted gradient echo image of cell samples acquired at $100 \times 100 \times 200$ μm^3 spatial resolution, with TE = 15 ms. Note the increase in contrast as cell concentration increases. (C, D) *Ex-vivo* T_2^*-weighted images of mouse brain ($75 \times 75 \times 75$ μm^3 resolution, TE = 15 ms), 2 h following intranasal administration of MPIO-labeled MSC at 10 d after HI (C) or sham-operation (D). (C) Arrows show signal contrast from MPIO-labeled MSCs surrounding damaged region (yellow dashed line). (E, F) Panorama of ipsilateral cortex from HI (E) or sham-operated (F) mice. Note the Dragon Green signal in (E). scale bar = 200 μm. (E′) Iba-1 (red) staining on sections from brain shown in (E). (F′) Insert of sham-operated mice. Blue = DAPI; scale bar = 20 μm.

in vitro with MRI. The results clearly showed that MPIO signal intensity correlated with MSC concentration (Fig. 3B).

MPIO-labeled MSCs were administered to both nostrils 10 days post-HI or sham-operation and mice were sacrificed 2 h later. Hypo-intensities in T_2^*-weighted images were detected specifically in regions adjacent to the lesion site (Fig. 3C). No hypo-intensities were observed in the brains of sham-operated mice (Fig. 3D). To validate the MRI results, we analyzed brain sections for Dragon Green fluorescence. In the HI-injured brain we observed a strong fluorescent signal clustered in the somatosensory cortex adjacent to the lesion, in a pattern comparable to the MPIO signal observed with MRI (Fig. 3E). In agreement with our MRI results, no Dragon Green signal was observed in brains from sham-operated mice (Figs. 3F, F′).

To control for the possibility that dying MPIO-labeled MSCs or free MPIO had been taken up by microglia *in vivo*, we also analyzed colocalization of Iba-1 and Dragon Green. The results show that Iba-1^+ cells surround the Dragon Green fluorescent signal without overlapping (Fig. 3E′).

Neurotrophic factor expression by MSCs

To determine whether the HI brain environment stimulates MSCs to express the neurotrophic factors BDNF and NGF, we co-cultured MSCs with HI or sham-operated brain extracts from 10 days post-insult. Our results show that BDNF mRNA expression significantly increases after co-culture with HI brain extract, but not with sham-operated brain extract (Fig. 4C). NGF gene expression increased after co-culture with both HI and sham brain extracts (Fig. 4C).

Characterization of the early regenerative niche at the lesion

To characterize the cellular environment surrounding the MSCs at the lesion site, we stained ipsilateral brain sections at 1 day after MSC-treatment for NeuN, GFAP and Iba-1. PKH-26^+-MSCs were primarily surrounded by Iba-1^+ cells (Fig. 4A). $NeuN^+$ cells were found scattered around the MSCs. $GFAP^+$ cells formed a boundary border around the

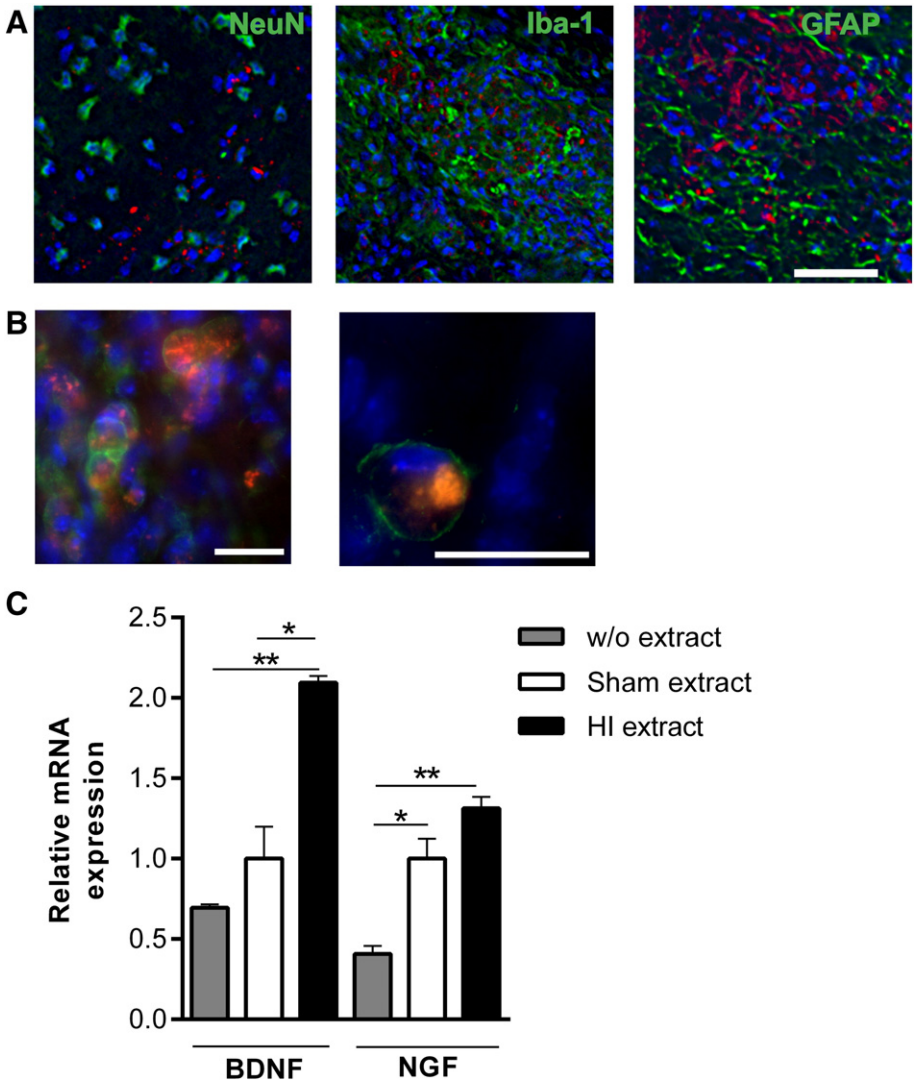

Fig. 4. Characterization of the cellular niche at the lesion and neurotrophic factor expression by MSCs. (A) Brain sections from 24 h after MSC-treatment were stained for NeuN (green), Iba-1 (green) and GFAP (green) expression. (n = 3 per group); red = PKH-26; blue = DAPI; scale bar = 50 μm. (B) Overlap between Iba-1$^+$ cells and PKH-26$^+$ signal at 2 h after MSC administration. Green = Iba-1; red = PKH-26; scale bar = 20 μm. (C) Relative mRNA expression of BDNF and NGF by MSCs at 72 h after co-culture without brain extract or with either HI or sham-operated brain extract (n = 2). Data represent mean ± SEM. * $p < 0.05$; **$p < 0.01$ by unpaired two-tailed T-test.

PKH-26$^+$-MSCs. There was no overlap between PKH-26$^+$ MSCs and NeuN$^+$, GFAP$^+$ or Iba-1$^+$ cells at 1 day. To determine whether Iba-1$^+$ cells overlapped with PKH-26$^+$-MSCs at an earlier time-point, we stained brain sections at 2 h following MSC-treatment for Iba-1. At this early time-point, we estimate that around 80% of the Iba-1$^+$ cells overlapped with the PKH-26$^+$-MSC-derived signal suggesting that Iba-1$^+$ cells may phagocytose dying MSCs (Fig. 4B).

MSCs increase the number of DCX$^+$ cells in the SVZ

First, we investigated whether MSCs affect neurogenesis in the SVZ. To this end, we assessed the number of neuronally-committed type A progenitor cells, *i.e.* neuroblasts, which have the phenotype of young migrating neurons. Coronal sections from the SVZ were stained for doublecortin (DCX) at 1, 3 and 5 days after MSC- or vehicle-treatment. MSC administration significantly increased the number of DCX$^+$ cells in the SVZ at 1 and 3 days (Figs. 5A–C). At 5 days after MSC-treatment, the number of DCX$^+$ cells had returned to the level observed in sham-operated mice (Fig. 5D). DCX$^+$ cell numbers increased in the contralateral SVZ at 1 day. HI alone did not lead to a significant increase in the number of DCX$^+$ cells at any of the time-points measured (Fig. 5).

Early effect of MSCs on neural progenitor cells at the lesion

Next, we determined the number of type B precursor cells (*i.e.* uncommitted precursors) at the lesion site, by quantifying the expression of GFAP$^+$/nestin$^+$ pixels in 10 fields, at 1, 3 and 5 days after MSC or vehicle administration (Fig. 6A). Our results show that the number of GFAP$^+$/nestin$^+$ pixels at 1 day after MSC-treatment is almost two times higher than in HI-Vehicle or sham-operated animals (Figs. 6B, C). At 5 days the amount of GFAP$^+$/nestin$^+$ pixels had returned to sham level. HI only led to a small significant increase in GFAP$^+$/nestin$^+$ expression on day 3. In sham-operated mice, GFAP$^+$/nestin$^+$ expression remained stable over time. In HI-Vehicle and HI-MSC animals, GFAP$^+$/nestin$^+$ cells were located at the lesion border. These data show that MSC enhance the number of type B precursor cells at the lesion, which suggests the formation of a neurogenic niche.

Next, we quantified the number of DCX$^+$ cells at the lesion. At both 1 and 3 days after MSC-treatment there was a significant increase in DCX$^+$ cells in the corpus callosum, and in the ipsilateral cortical and thalamic regions adjacent to the lesion (Figs. 7A, C). At 5 days, the number of DCX$^+$ cells in the ipsilateral hemisphere had returned to sham level (Figs. 7A, D). However, at this time-point the number of DCX$^+$ cells in

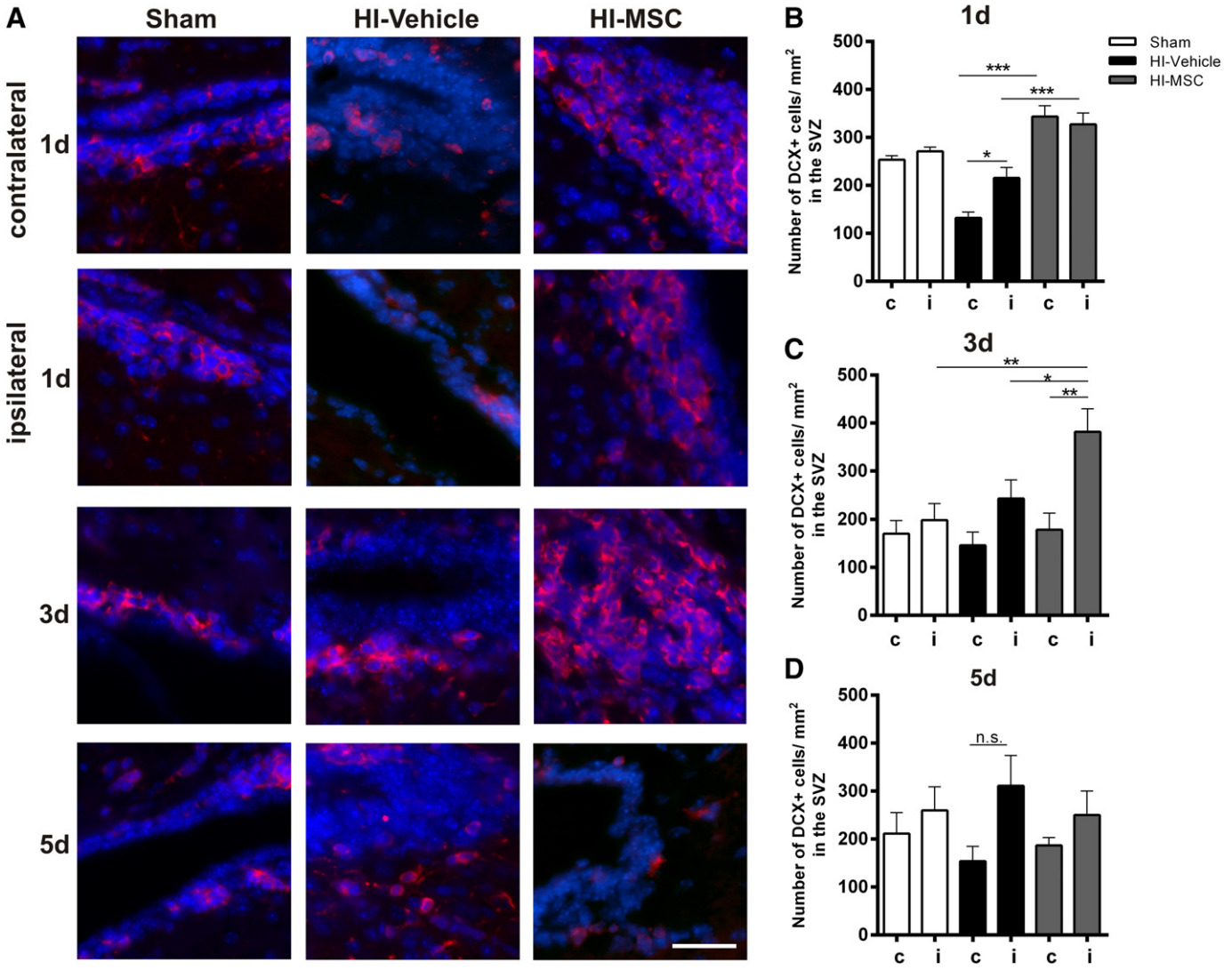

Fig. 5. MSCs increase the expression of DCX in the SVZ. DCX expression in the SVZ at 1, 3 and 5 d after MSC or vehicle administration and in sham-operated brain. (A) Representative images of sham, HI-Vehicle or HI-MSC at 1, 3 and 5 d after treatment. (B–D) Quantification of DCX^+ cells in the contra- and ipsilateral SVZs at 1 d (B), 3 d (C) and 5 d (D). Data represent mean ± SEM. $^*p < 0.05$; $^{**}p < 0.01$; $^{***}p < 0.001$; n.s. = not significant by ANOVA and Bonferroni post-hoc test (n = 6 per group). Red = DCX; blue = DAPI; scale bar = 32 μm.

the ipsilateral hemisphere of MSC-treated mice was significantly higher than in the contralateral area (Fig. 7D). In HI-Vehicle mice, DCX expression at the lesion or contralateral side was not changed at 1 to 5 days (*i.e.* 11–15 days post-HI) (Fig. 7). DCX expression remained constant in sham-operated mice. These results demonstrate that MSCs also enhance the number of neuronally-committed progenitor cells at the lesion.

MSCs regenerate the lesioned brain

Next, we investigated whether MSC-treatment leads to increased repopulation of lost brain structures. We determined the number of $NeuN^+$ cells in the damaged somatosensory cortex and hippocampus at 1, 5 and 18 days after MSC- or vehicle-treatment. Our results show a significant loss of tissue, encompassing the hippocampus and somatosensory cortex, which can be clearly discerned as a cavity at 11 days after HI (*i.e.* 1 day after MSC- or vehicle-treatment) (Fig. 8A). In HI-Vehicle mice this cavity was still discernible at 18 days (Fig. 8A). The lesion in the somatosensory region was repopulated by $NeuN^+$ cells at 5 days following MSC-treatment, and the number of neurons had significantly increased compared to HI-Vehicle mice, and reached sham-level (Figs. 8B, C). At 18 days after MSC-treatment, NeuN expression in the somatosensory cortex was still increased. At 5 days following MSC-treatment, an area with hippocampal morphology started to emerge (Fig. 8D). At this time point, $NeuN^+$ cells repopulated the dentate gyrus and we also observed a partial recovery of the CA1, CA2 and CA3 regions. At 18 days, the dentate gyrus, CA1, CA2 and CA3 regions had further regenerated and the hippocampal structure was clearly discernible (Fig. 8D).

Effect of MSCs on astrocyte and microglia activation

To assess whether MSC-treatment has an effect on the number of astrocytes and microglia, we quantified expression of $GFAP^+$ and Iba-1^+ cells at 1, 5 and 18 days after MSC- or vehicle-treatment. Figs. 9A and B show that the number of microglia and astrocytes are substantially upregulated at the lesion at all time-points. Following HI, Iba-1^+ cells show morphological characteristics that correlate with an activated state (amoeboid phenotype) (Fig. 9A). $GFAP^+$ cells change their star shape morphology to a more rounded, multipolar morphology. A dense network of reactive astrocytes demarcates the entire lesion (Fig. 9B). At 1 day after MSC-treatment, no significant difference in

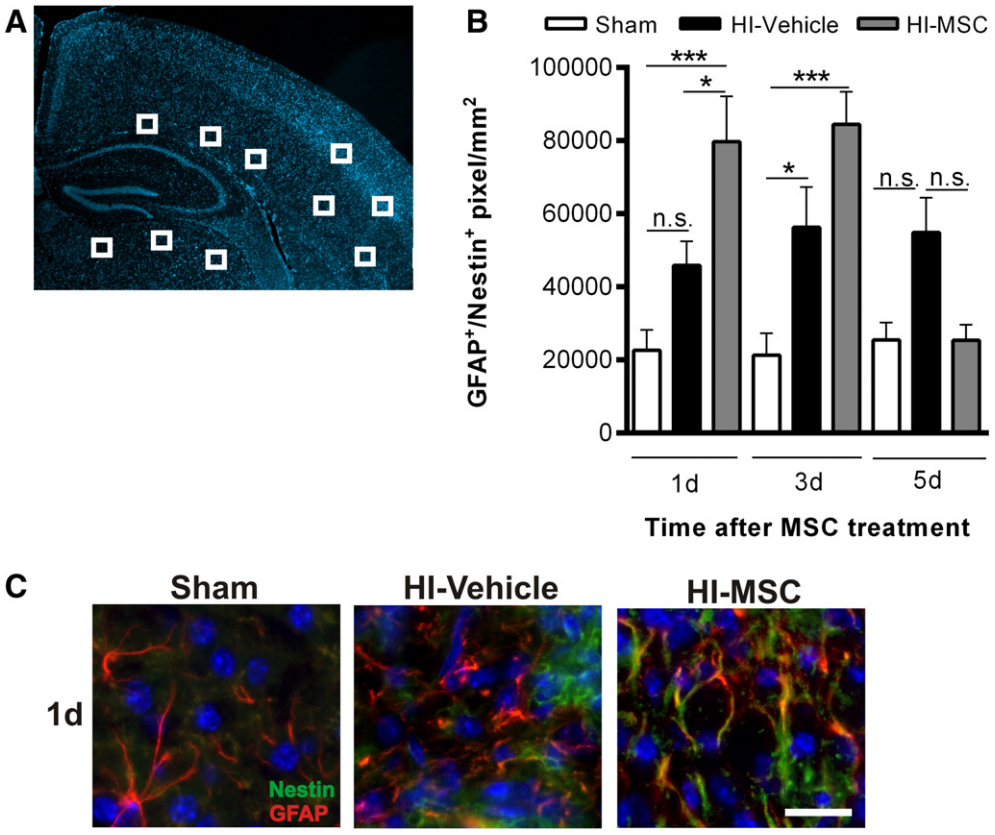

Fig. 6. Expression of neural precursor cells increases following MSC-treatment. GFAP and nestin expression at the lesion site at 1, 3 and 5 d after MSC or vehicle treatment and in sham-operated brain. (A) Schematic illustration of regions that were quantified. (B) Quantification of GFAP$^+$/nestin$^+$ pixels at 1, 3 and 5 d. (C) Representative images of sham, HI-Vehicle or HI-MSC at 1 d after treatment. Data represent mean ± SEM. *$p < 0.05$; ***$p < 0.001$; n.s. = not significant by ANOVA and Bonferroni post-hoc test (n = 6 per group). Green = Nestin; red = GFAP; blue = DAPI; scale bar = 20 μm.

either Iba-1$^+$ or GFAP$^+$ expression was observed between vehicle- and MSC-treated mice (Figs. 9A, B). However, at 18 days following MSC-treatment, GFAP and Iba-1 expression levels are substantially decreased compared to levels in vehicle-treated HI mice and have returned to sham level (Figs. 9A, B).

Polarization of microglial cells following MSC-treatment

As microglia can have distinct phenotypes, *e.g.* pro-inflammatory (M1) or regenerative/anti-inflammatory (M2a/b), we assessed whether MSC-treatment affects microglia polarization. We double-stained coronal sections for CD16/32 (M1) or CD206 (M2) and Iba-1. Our data show that HI-Vehicle mice have a higher expression of both M1 and M2 microglia than sham-operated mice, but no significant polarization towards the M1 or the M2 phenotype (Figs. 9C, D). MSC-treatment induced polarization towards the M2 phenotype.

Discussion

In view of the pre-clinical efficacy of MSC-treatment and the lack of effective therapies for infants with neonatal brain damage, intranasal MSC administration might become a powerful therapeutic strategy in the future. In previous studies we described the potent effect that MSCs have in decreasing lesion size and improving motor and cognitive behavior following HI injury (Donega et al., 2013a; van Velthoven et al., 2010, 2011, 2013). Yet, how MSCs mediate this effect is unclear. Here, we describe the effect of intranasally administered MSCs on the cellular composition of the 'regenerative niche' in the SVZ and lesion. Moreover, we followed repair of the lesion by quantifying the number of GFAP$^+$/nestin$^+$, DCX$^+$ and NeuN$^+$ cells, astrocytes and microglia until 18 days after MSC-treatment (*i.e.* 28 days post-HI). Following application of MSCs, cells migrate from the ipsi- and contralateral nasal cavities to the unilateral lesion within 2 h after administration. The number of MSCs decreases sharply at 72 h, which is in accordance with previous findings (van Velthoven et al., 2011). This indicates that MSCs *induce* a cascade of events leading to tissue repair. MSCs not only increase the number of GFAP$^+$/nestin$^+$ and DCX$^+$ cells at the lesion within 1 day after intranasal administration, but also induce maturation of neuroblasts following HI brain injury (Fig. 10). Moreover, MSCs induce microglial polarization towards a M2 phenotype and decrease the number of activated astroglial cells at 18 days after treatment. Our key finding is that intranasal MSC-treatment leads to a remarkably fast regeneration of the lesion, as repopulation of the somatosensory and hippocampal regions starts within 5 days after administration.

The MSC signal detected with MRI and Dragon Green fluorescence surrounding the lesion at 2 h after administration (Fig. 3) closely resembles the PKH-26$^+$ MSC signal, which forms clusters alongside the lesion (Fig. 2). We checked for the possibility that MPIOs are phagocytosed by microglia, thereby leading to false positive results. However, Iba-1 staining showed no overlap with the MPIO-labeled MSCs, further supporting that the MRI signal and the Dragon Green fluorescence correspond to the presence of MSCs at the lesion. Yet, at 2 h after MSC administration, around 80% of the PKH26$^+$ signal overlapped with Iba-1$^+$ microglia (Fig. 4B). In contrast, at 1 day there was no overlap between the Iba-1$^+$ signal and the PKH26$^+$ signal (Fig. 4A). To explain the apparent discrepancy between results we postulate that the first MSCs reaching the lesion at 2 h will be phagocytosed by activated microglia, which may in turn affect the local brain environment that will shift towards an environment more receptive for MSCs. Hence, at 12 h, when there is a peak in the number of MSCs in the lesion, the environment is more receptive to the MSCs, which are no longer phagocytosed. The fact that we

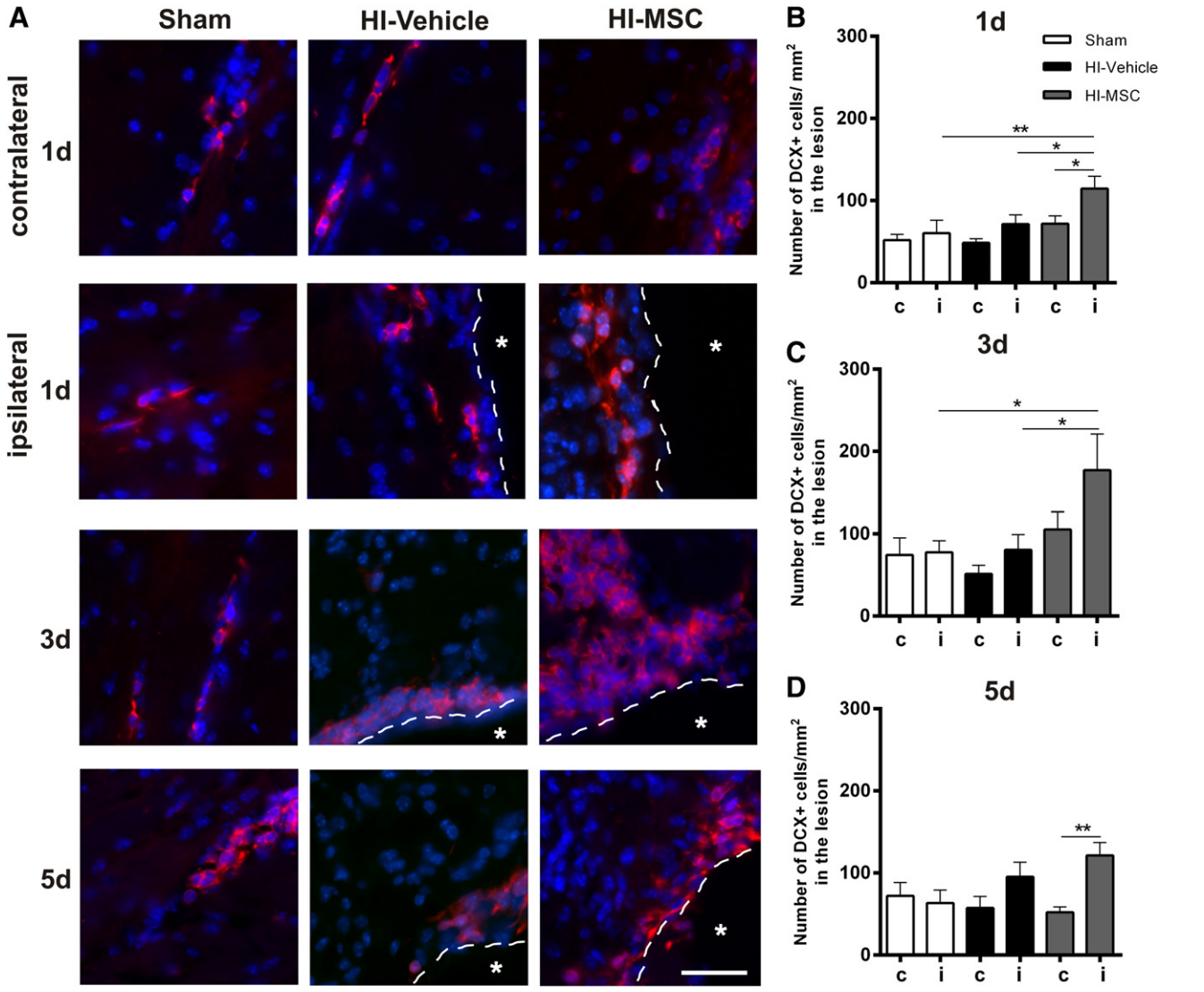

Fig. 7. DCX expression is increased at the lesion site following MSC-treatment. DCX expression at the lesion at 1, 3 and 5 d after MSC or vehicle administration and in sham-operated brains. (A) Representative images of sham, HI-Vehicle or HI-MSC at 1, 3 and 5 d after treatment. (B–D) Quantification of DCX^+ cells adjacent to the lesion and at the undamaged contralateral side at 1 d (B), 3 d (C) and 5 d (D). Data represent mean ± SEM. *$p < 0.05$; **$p < 0.01$ by ANOVA and Bonferroni post-hoc test ($n = 6$ per group). Red = DCX; blue = DAPI; asterisk = lesion; dashed line = lesion border. scale bar = 32 μm.

did not observe an overlap between Dragon Green signal and the Iba-1^+ signal at 2 h after MSC administration might be due to the relatively strong Dragon Green staining (Fig. 3E′).

Our finding that MSCs reach the damaged area within 2 h makes it unlikely that MSCs migrate to the lesion through the brain parenchyma. Neural precursor cells have been shown to migrate 94 μm ± 20 μm per hour along the rostral migratory stream (RMS) (Murase and Horwitz, 2002). Hence, if one would assume that MSCs migrate at a similar rate it would take several days to reach the damaged region. Therefore, it seems more plausible that MSCs migrate from the intranasal cavity towards the lesion through the meningeal circulation or along blood vessels in the lamina propria or *via* the cerebral spinal fluid.

In order to study whether MSCs increase the number of neuronally-committed cells in the neurogenic niche in the SVZ, we determined the presence of DCX^+ cells in the SVZ. We show that MSCs increase the number of neuroblasts in the ipsilateral SVZ at 1 and 3 days after treatment (Fig. 5). As we did not find MSCs in the SVZ region at any time-point, we postulate that MSCs at the lesion induce neurotrophic factor production in the SVZ, possibly through paracrine signaling by MSCs, which in turn promotes differentiation of type B precursor cells towards neuroblasts in the SVZ. The fact that most of the increase in DCX^+ cells in the SVZ was detected in the ipsilateral side indicates that MSC presence at the lesion leads to increased precursor cells in the SVZ. These results raise the interesting possibility that neuroblasts in the SVZ may migrate towards the lesion to repopulate the damaged cortical areas (Inta et al., 2008; Kempermann et al., 2004; Zhao et al., 2008).

Anderova et al. (2011) described that HI increases the number of $GFAP^+$/$nestin^+$ NSCs in the hippocampus in adult rats. Neonatal HI has also been demonstrated to increase the number of neuroblasts in the lesion 1–3 weeks post-insult (Fagel et al., 2006; Felling et al., 2006; Kadam et al., 2008). We detected a small increase of $GFAP^+$/$nestin^+$ expression at the lesion at 3 days (*i.e.* 13 days post-HI) after vehicle-treatment. We did not observe any change in DCX expression after vehicle-treatment. Therefore, we conclude from our data that neurogenesis is impaired following neonatal HI, which is in accordance with current literature (Donega et al., 2013b). In contrast, 1 day after MSC-treatment, the number of $GFAP^+$/$nestin^+$ cells surrounding the lesion had increased almost two times in comparison to HI-Vehicle mice (Fig. 6). At 5 days after MSC administration the number of precursor cells had returned to sham level. Moreover, we found a substantial increase in DCX^+ cells at 1 and 3 days after MSC, which declined to sham level at 5 days (Fig. 7).

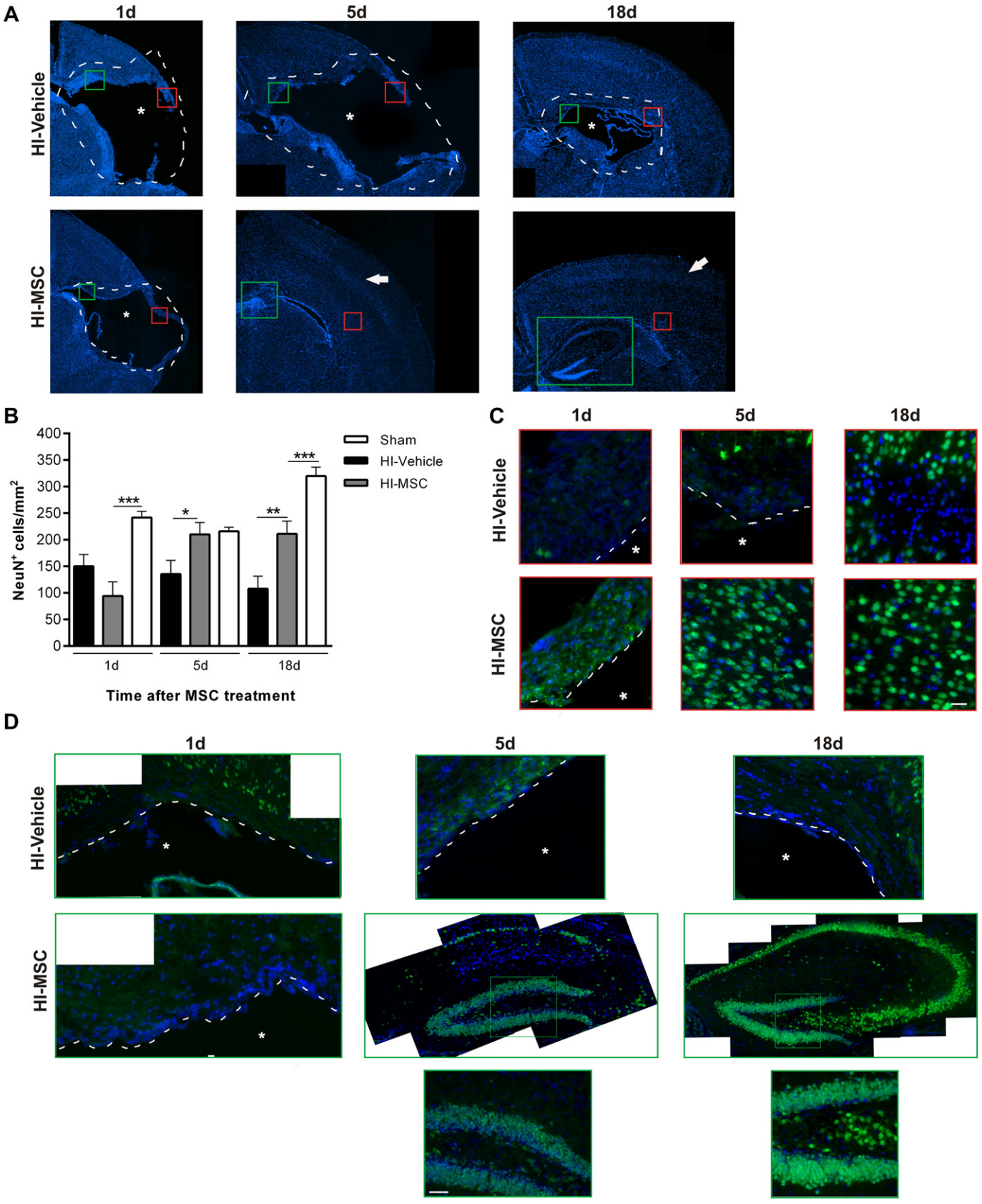

Fig. 8. Regeneration following MSC administration. NeuN expression at 1, 5 and 18 d following vehicle or MSC administration. (A) Overview of the macroscopic lesion site at 1, 5 and 18 d after vehicle or MSC-treatment. Note cortical Layer 4 (arrow) at 5 and 18 d after MSC-treatment. Red square = insert shown in (C); green square = insert shown in (D). (B) Quantification of $NeuN^+$ cells in 4 random fields in the ipsilateral somatosensory cortex. (C) Representative images of NeuN expression in the somatosensory cortex of HI-Vehicle and HI-MSC. (D) Representative images of NeuN expression in the hippocampal structure at 1, 5 and 18 d following MSC or vehicle-treatment. Data represent mean ± SEM. $^*p < 0.05$; $^{**}p < 0.01$; $^{***}p < 0.001$ by ANOVA and Bonferroni post-hoc test (n = 6 per group). green = NeuN; blue = DAPI; Asterisk = lesion site; Dashed line = boundary lesion. scale bar = 50 μm in C, D.

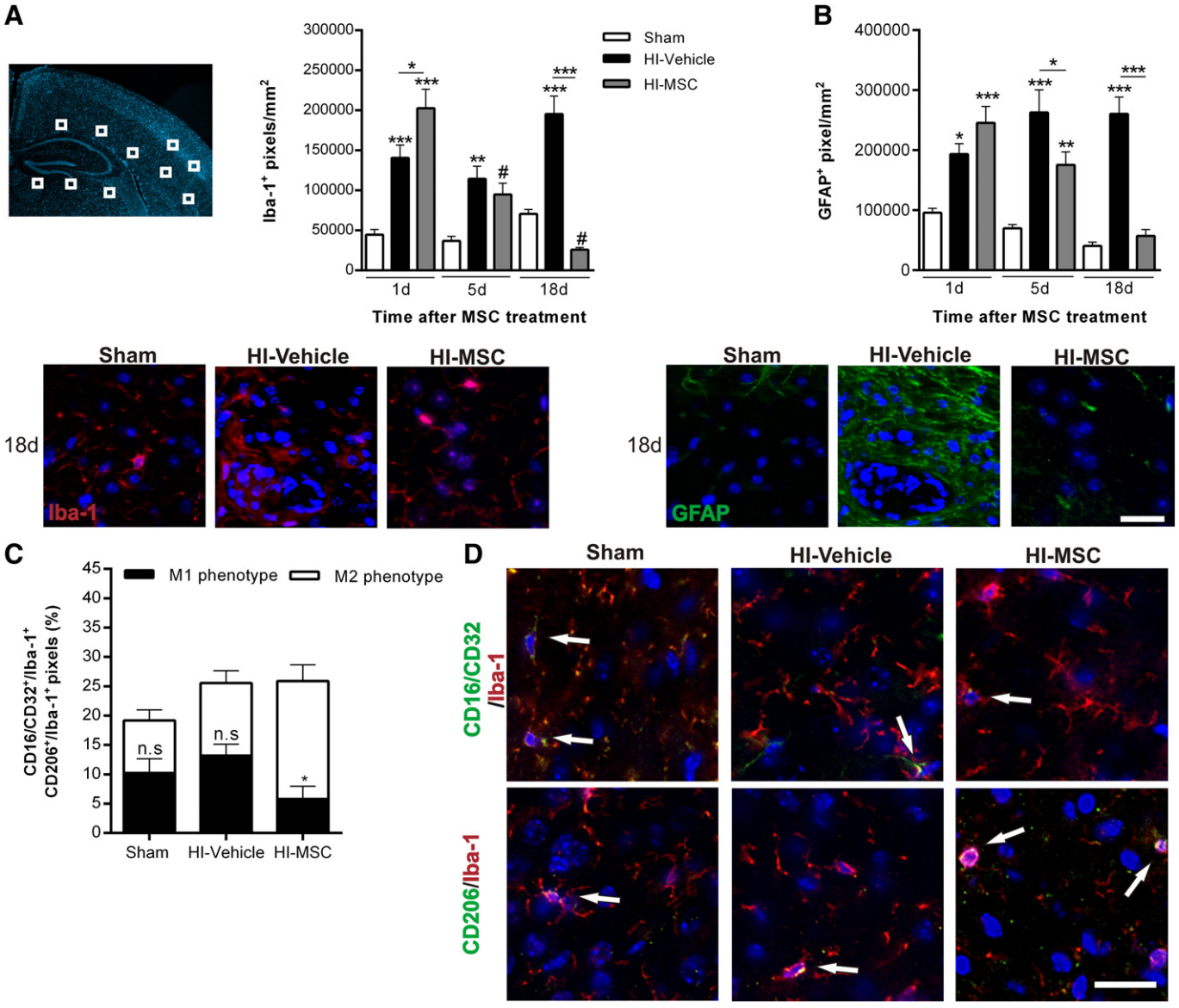

Fig. 9. MSCs revert astrogliosis at the damaged region. Iba-1 and GFAP expression at the lesion at 1, 5 and 18 d after MSC or Vehicle administration. (A) Upper: Quantification of Iba-1$^+$ at 1, 5 and 18 d and a schematic view of the regions that were quantified in (A), (B) and (C). Lower: Representative images of Iba-1$^+$ cells in sham, HI-Vehicle and HI-MSC at 18 d. (B) Upper: Quantification of GFAP$^+$ pixels at 1, 5 and 18 d. Lower: Representative images of GFAP$^+$ cells in sham, HI-Vehicle and HI-MSC at 18 d. (C) Quantification of CD16/32$^+$/Iba-1$^+$ pixels and CD206$^+$/Iba-1$^+$ pixels at 5 d. (D) Representative images of CD16/32$^+$/Iba-1$^+$ cells and CD206$^+$/Iba-1$^+$ cells at 5 d after MSC-treatment. Data represent mean ± SEM. (A, B). *$p < 0.05$; **$p < 0.01$; ***$p < 0.001$; # = not significant for sham 5 d vs HI-MSC 5 d and sham 18 d vs HI-MSC 18 d by ANOVA and Bonferroni post-hoc test. (C) *$p < 0.05$ by multiple T-test corrected with the Holm–Sidak method (n = 6 per group). Red = Iba-1 (A, D); green = GFAP (B), CD206, CD16/CD32 (D); blue = DAPI; scale bar = 20 μm.

Our results show that this increase in the number of DCX$^+$ cells was short-lasting as at 5 days after MSC administration it had returned to sham level suggesting that the DCX$^+$ cells had either differentiated to a more mature phenotype or died. As GFAP$^+$/nestin$^+$ cells first become nestin$^+$ before differentiating towards DCX$^+$ cells, we also investigated whether the GFAP$^+$/nestin$^+$ cells had differentiated towards the nestin$^+$ intermediate phenotype at 5 days. We found that at 5 days, nestin$^+$ cells are still significantly increased in the lesion in comparison to sham, which suggests that the GFAP$^+$/nestin$^+$ cells have become type 2 precursor cells at 5 days (data not shown). These data suggest that the differentiation of nestin$^+$ cells into adult neurons and astrocytes may continue after 5 days following MSC treatment.

Next, we investigated whether the DCX$^+$ cells had further differentiated into more mature neurons, by assessing the number of NeuN$^+$ cells after MSC- and vehicle-treatment. Our results show extensive tissue loss encompassing the somatosensory cortex and hippocampus 1 day (*i.e.* 11 days post-HI) following vehicle- or MSC-treatment. Furthermore, we observed that in the vehicle-treated mice the lesion size did not aggravate any further after 11 days post-HI. However, at 5 days after MSC-treatment the number of NeuN$^+$ cells increases significantly reaching sham level. These NeuN$^+$ cells will repopulate the damaged somatosensory cortex resulting in cortical lamination as Layer 4 can be clearly distinguished (Figs. 8A–C). The hippocampal region also starts to regenerate at 5 days after MSC-treatment. The dentate gyrus is well defined and the CA1, CA2 and CA3 regions are beginning to repopulate. The CA1, CA2 and CA3 regions develop further at 18 days. The fact that at 10 days post-HI, there is significant tissue loss and the lesion does not augment, does not support a neuroprotective role for MSCs in our model. Instead, the results strongly support that MSC induced lesion repair is due to increased neuroregeneration.

MSCs are known to have a strong immunomodulatory capacity and to decrease inflammatory responses following injury (Tse et al., 2003;

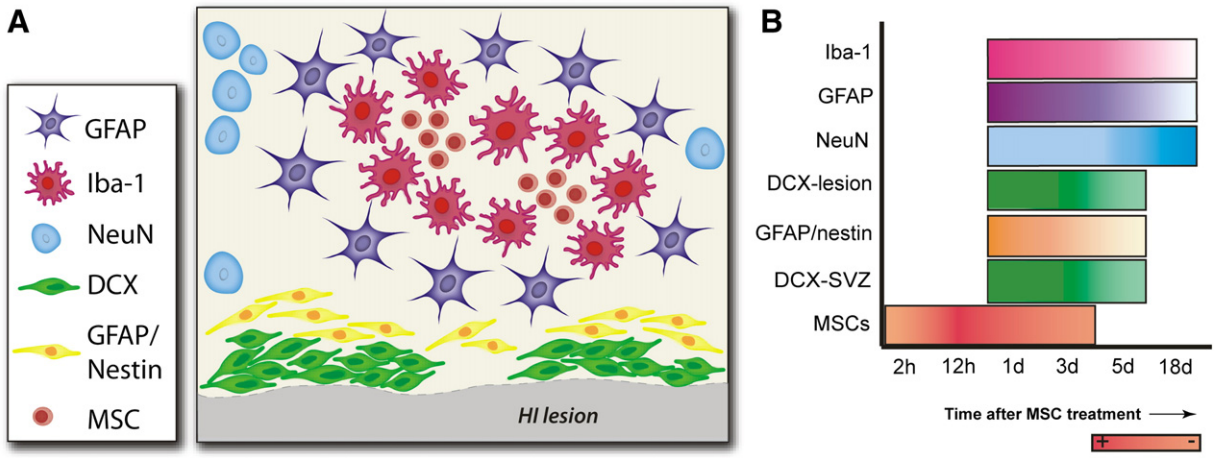

Fig. 10. Schematic overview of location and changes in number of MSCs, precursor cells and glial cells. (A) Schematic figure showing location of MSCs, GFAP$^+$/nestin$^+$, DCX$^+$, GFAP$^+$ and Iba-1$^+$ cells at the lesion at 1 d after administration. (B) Diagram depicting changes in MSC, GFAP/nestin, DCX, NeuN, GFAP and Iba-1 expression over time.

Salem and Thiemermann, 2010; Zhang et al., 2013). Astrocytes have been shown to be a (functionally) heterogeneous cell population that can be either detrimental to neurogenesis or supportive of neuronal function (Garcia et al, 2004, Rusnakova et al., 2013; Salem and Thiemermann, 2010; Sofroniew, 2013). Whether astrocytes will lead to astrogliosis and impair regeneration or promote neurogenesis and repair, depends on a plethora of signals including pro-inflammatory (*e.g.* IFN-γ and IL-1) and damage signals (*e.g.* DAMPs and PAMPs) (Sofroniew, 2013). At 1 day after vehicle- or MSC-treatment we observed a significant amount of GFAP$^+$ cells surrounding the lesion. Interestingly, 18 days after MSC-treatment the amount of GFAP$^+$ expressing cells had decreased back to sham level (Fig. 9), which suggests that MSCs may also decrease gliosis, since in HI-Vehicle animals there is still a dense network of reactive astrocytes at the lesion border.

Microglia, like astrocytes, can have either a pro-inflammatory effect (M1) or promote tissue repair and anti-inflammation (M2) (Chor et al., 2013; Czeh et al., 2011; Neumann et al., 2006; Wake et al., 2013). We show that MSCs stimulate microglia polarization towards a M2 phenotype (Fig. 9). This may be mediated by the immunosuppressive effects of MSCs. In this respect, it is of interest that we have shown increased IL-10 mRNA expression after MSC transplantation (van Velthoven et al., 2011). MSC-treatment decreases the number of microglia at 28 days after HI, the time-point when repair of the lesion by NeuN$^+$ cells was observed. These findings suggest that lesion repair is associated with an anti-inflammatory environment and that the immunosuppressive capacity of MSCs play an important role in mediating regeneration following HI injury (Kokaia et al., 2012).

In conclusion, the results in this study demonstrate that intranasal MSCs decrease lesion volume by promoting formation of a 'neurogenic niche' leading to a dramatic reconstruction of the hippocampus and somatosensory cortex (Fig. 8). This is crucial as the regenerative signal induced by HI is largely insufficient (Donega et al., 2013b). Our present study demonstrates that MSCs boost the endogenous regenerative capacity by promoting neurogenesis and neuronal survival. Importantly, we show evidence that MSCs are directly involved in inducing and supporting a shift to a neurogenesis supportive environment, as we found that MSCs express more BDNF following contact with a HI environment. Co-culture of MSCs with brain extract from sham-operated mice doubles the mRNA expression of NGF. In contrast to BDNF, co-culture with HI brain extract does not further increase the production of NGF. This may suggest that factors present in the brain of sham animals stimulate MSCs to maintain production of NGF. Following injury, endogenous stimuli in the brain will increase the production of BDNF by MSCs to promote neurogenesis. Therefore, this suggests that the HI brain environment stimulates MSCs to secrete specific neurotrophic factors (see also Supplemental Fig. 1). The neurotrophic factor BDNF plays an important role in proliferation, migration, differentiation and survival of neuronal cells (Yuan, 2008). Moreover, we have previously shown that intracranially-administered MSCs upregulate gene expression of several neurotrophic factors (van Velthoven et al., 2011). Both the SVZ and lesion site may be sources of progenitor cells. MSCs may induce migration of DCX$^+$ cells from the SVZ to the lesion and also stimulate a subset of reactive astrocytes in the lesion to develop stem cell potential. MSCs also revert scar formation, which is known to impair neurogenesis. These findings are of clinical importance as they further delineate the power of MSCs as a future therapeutic strategy for neonatal HI brain damage.

Supplementary data to this article can be found online at http://dx.doi.org/10.1016/j.expneurol.2014.06.009.

Role of the funding source

This study was supported by Zon-MW Project (no 116002003) and EU-7 Neurobid (HEALTH-F2-2009-241778) from the European Union.

References

Anderova, M., Vorisek, I., Pivonkova, H., et al., 2011. Cell death/proliferation and alterations in glial morphology contribute to changes in diffusivity in the rat hippocampus after hypoxia–ischemia. J. Cereb. Blood Flow Metab. 31, 894–907.
Bacigaluppi, M., Pluchino, S., Jametti, L.P., et al., 2009. Delayed post-ischaemic neuroprotection following systemic neural stem cell transplantation involves multiple mechanisms. Brain 132, 2239–2251.
Chor, V., Charpentier, T.L., Lebon, S., et al., 2013. Characterization of phenotype markers and neuronotoxic potential of polarized primary microglia in vitro. Brain Behav. Immun. 32, 70–85.
Crigler, L., Robey, R.C., Asawachaicharn, A., et al., 2006. Human mesenchymal stem cell subpopulations express a variety of neuro-regulatory molecules and promote neuronal cell survival and neuritogenesis. Exp. Neurol. 198, 54–64.
Czeh, M., Gressens, P., Kaindl, A.M., 2011. The Yin and Yang of microglia. Dev. Neurosci. 33, 199–209.
Daadi, M.M., Davis, A.S., Arac, A., et al., 2010. Human neural stem cells grafts modify microglial response and enhance axonal sprouting in neonatal hypoxic–ischemic brain injury. Stroke 41, 516–523.
De Haan, M., Wyatt, J.S., Roth, S., et al., 2006. Brain and cognitive-behavioural development after asphyxia at term birth. Dev. Sci. 9, 350–358.
Donega, V., van Velthoven, C.T., Nijboer, C.H., et al., 2013a. Intranasal mesenchymal stem cell treatment for neonatal brain damage: long-term cognitive and sensorimotor improvement. PLoS One 8, e51253.
Donega, V., Velthoven, C., Nijboer, C.H., et al., 2013b. The endogenous regenerative capacity of the damaged newborn brain: boosting neurogenesis with mesenchymal stem cell treatment. J. Cereb. Blood Flow Metab. 33, 625–634.
Fagel, D.M., Ganat, Y., Silbereis, J., et al., 2006. Cortical neurogenesis enhanced by chronic perinatal hypoxia. Exp. Neurol. 199, 77–91.
Felling, R.J., Snyder, M.J., Romanko, M.J., et al., 2006. Neural stem/progenitor cells participate in the regenerative response to perinatal hypoxia–ischemia. J. Neurosci. 26, 4359–4369.

Ferriero, D.M., 2004. Neonatal brain injury. N. Engl. J. Med. 351, 1985–1995.
Garcia, D.R., Doan, N.B., Imura, T., et al., 2004. GFAP-expressing progenitors are the principal source of constitutive neurogenesis in adult mouse forebrain. Nat. Neurosci. 7, 1233–1241.
Graham, E.M., Ruis, K.A., Hartman, A.L., et al., 2008. A systematic review of the role of intrapartum hypoxia–ischemia in the causation of neonatal encephalopathy. Am. J. Obstet. Gynecol. 199, 587–595.
Inta, D., Alfonso, J., von Engelhardt, et al., 2008. Neurogenesis and widespread forebrain migration of distinct GABAergic neurons from postnatal subventricular zone. Proc. Natl. Acad. Sci. U. S. A. 105, 20994–20999.
Kadam, S.D., Mulholland, J.D., McDonald, J.W., et al., 2008. Neurogenesis and neuronal commitment following ischemia in a new mouse model for neonatal stroke. Brain Res. 1208, 35–45.
Kempermann, G., Jessberger, S., Steiner, B., et al., 2004. Milestones of neuronal development in the adult hippocampus. Trends Neurosci. 27, 447–452.
Kokaia, Z., Martino, G., Schwartz, M., et al., 2012. Cross-talk between neural stem cells and immune cells: the key to better brain repair? Nat. Rev. Neurosci. 15, 1078–1087.
Lee, J.A., Kim, B.I., Jo, C.H., et al., 2010. Mesenchymal stem cell transplantation for hypoxic–ischemic brain injury in a neonatal rat model. Pediatr. Res. 67, 42–46.
Murase, S.I., Horwitz, A.F., 2002. Deleted in colorectal carcinoma and differentially expressed integrins mediate the directional migration of neural precursors in the rostral migratory stream. J. Neurosci. 22, 3568–3579.
Neumann, J., Gunzer, M., Gutzeit, H.O., et al., 2006. Microglia provide neuroprotection after ischemia. FASEB J. 20, 714–720.
Pimentel-Coelho, P.M., Magalhaes, E.S., Lopes, L.M., et al., 2010. Human cord blood transplantation in a neonatal rat model of hypoxic–ischemic brain damage: functional outcome related to neuroprotection in the striatum. Stem Cells Dev. 19, 351–358.
Rusnakova, V., Honsa, P., Dzamba, D., et al., 2013. Heterogeneity of astrocytes: from development to injury-single cell gene expression. PLoS One 8, e69734.
Salem, H.K., Thiemermann, C., 2010. Mesenchymal stromal cells: current understanding and clinical status. Stem Cells 28, 585–596.
Sofroniew, M.V., 2013. Multiple roles for astrocytes as effectors of cytokines and inflammatory mediators. Neuroscientist 20, 160–172.
Titomanlio, L., Kavelaars, A., Dalous, J., et al., 2011. Stem cell therapy for neonatal brain injury: perspectives and challenges. Ann. Neurol. 70, 698–712.
Tse, W.T., Pendlenton, J.D., Beyer, W.M., et al., 2003. Suppression of allogeneic T-cell proliferation by human marrow stromal cells: implications in transplantation. Transplantation 75, 389–397.
Van Handel, M., Swaab, H., de Vries, L.S., et al., 2007. Long-term cognitive and behavioural consequences of neonatal encephalopathy following perinatal asphyxia: a review. Eur. J. Pediatr. 166, 645–654.
van Velthoven, C.T., Kavelaars, A., van Bel, F., et al., 2010. Repeated mesenchymal stem cell treatment after neonatal hypoxia–ischemia has distinct effects on formation and maturation of new neurons and oligodendrocytes leading to restoration of damage, corticospinal motor tract activity, and sensorimotor function. J. Neurosci. 30, 9603–9611.
van Velthoven, C.T., Kavelaars, A., van Bel, F., et al., 2011. Mesenchymal stem cell transplantation changes the gene expression profile of the neonatal ischemic brain. Brain Behav. Immun. 25, 1342–1350.
van Velthoven, C.T., Braccioli, L., Willemen, H.L., et al., 2013. Therapeutic potential of geneticaly modified mesenchymal stem cells after neonatal hypoxic–ischemic brain damage. Mol. Ther. 22, 645–654.
Volpe, J.J., 2001. Perinatal brain injury: from pathogenesis to neuroprotection. Ment. Retard. Dev. Disabil. Res. Rev. 7, 56–64.
Wake, H., Moorhouse, A.J., Miyamoto, A., et al., 2013. Microglia: actively surveying and shaping neuronal circuit structure and function. Trends Neurosci. 36, 209–217.
Yasahura, T., Hara, K., Maki, M., et al., 2008. Intravenous grafts recapitulate the neurorestoration afforded by intracerebrally delivered multipotent adult progenitor cells in neonatal hypoxic–ischemic rats. J. Cereb. Blood Flow Metab. 28, 1804–1810.
Yuan, T.F., 2008. BDNF signaling during olfactory bulb neurogenesis. J. Neurosci. 28, 5139–5140.
Zhang, R., Liu, Y., Yan, K., et al., 2013. Anti-inflammatory and immunomodulatory mechanisms of mesenchymal stem cell transplantation in experimental traumatic brain injury. J. Neuroinflammation 10, 106–118.
Zhao, C., Deng, W., Gage, F.H., 2008. Mechanisms and functional implications of adult neurogenesis. Cell 132, 645–660.